Pressure-induced insulator-to-metal transition in few-layer $FePS_3$ at 1.5 GPa

Bidyut Mallick,[1,*] Mainak Palit,[2,*] Rajkumar Jana,[3,*] Soumik Das,[2] Anudeepa Ghosh,[2] Janaky Sunil,[4] Sujan Maity,[2] Bikash Das,[2] Tanima Kundu,[2] Chandrabhas Narayana,[4] Ayan Datta,[3] and Subhadeep Datta[2,†]

[1]*Department of Applied Sciences and Humanities, Galgotias College of Engineering and Technology, Knowledge Park-II, Greater Noida, Uttar Pradesh 201310, India*

[2]*School of Physical Sciences, Indian Association for the Cultivation of Science, 2A & 2B Raja S. C. Mullick Road, Jadavpur, Kolkata 700032, India*

[3]*School of Chemical Sciences, Indian Association for the Cultivation of Science, 2A & 2B Raja S. C. Mullick Road, Jadavpur, Kolkata 700032, India*

[4]*Chemistry and Physics of Materials Unit, Jawaharlal Nehru Centre for Advanced Scientific Research, Jakkur P.O., Bangalore 560064, India*

(Received 20 March 2023; revised 1 May 2024; accepted 30 May 2024; published 14 June 2024)

In two-dimensional van der Waals (vdW) layered materials, application of pressure often induces a giant lattice collapse, which can subsequently drive an associated Mott transition. Here, we investigate room-temperature layer-dependent insulator-metal transition (IMT) and probable spin-crossover in vdW magnet, $FePS_3$, under high-pressure using micro-Raman scattering. Experimentally obtained spectra, in agreement with the computed Raman modes, indicate evidence of IMT of $FePS_3$ started with a thickness-dependent critical pressure (P_c) which reduces to 1.5 GPa in trilayer flakes compared with 10.8 GPa for the bulk counterpart. Using a phenomenological model, we argue that strong structural anisotropy in few-layer flakes enhances the in-plane strain under applied pressure and is, therefore, ultimately responsible for reducing the critical pressure for the IMT with decreasing layer numbers. Reduction of the critical pressure for phase transition in vdW magnets to 1–2 GPa marks the possibility of using intercalated few-layers in the field-effect transistor device architecture, and thereby, avoiding the conventional use of the diamond anvil cell.

DOI: 10.1103/PhysRevB.109.235417

I. INTRODUCTION

Correlation between electronic and magnetic properties in quantum materials can be realized in spatially confined two-dimensional (2D) flakes of van der Waals (vdW) magnets under high pressure. Moreover, with varying layer thickness, i.e.., reducing the flake thicknesses down to a few-atomic layers, electronic band structure and spin texture can be altered, as a result of which charge transport and magnetism can be controlled [1–6]. Stacking of isolated monolayers and multilayers of dissimilar materials led to the finding of vdW heterostructures and superlattices with exotic behavior resulting in practical electronic and spintronic devices [7,8]. Recently, the discovery of 2D long-range magnetic ordering and strong coupling in the spin-valley degree of freedom in 2D semiconductors has generated considerable interest because these materials would be an ideal building blocks to design multistate spin logic [9,10]. Furthermore, a 2D electronic system with quasi-one-dimensional triangular spin-lattice shows antiferromagnetic ordering at ambient pressure, but superconductivity under high pressure [11]. Even though theoretical studies have proposed a number of 2D magnets down to monolayer limit [12–16], very few experimental reports concern 2D flakes [17–20]. Thus, tunable spin-ordering in few-layer magnets in comparison to their bulk counterpart is important for exploring exotic phases in new device architecture. A substantial amount of work has been done on the magnetism of bulk 2D transition metal phosphorous trichalcogenide (MPX_3) materials [21]. The magnetization of these materials varies with the d-electron configurations of the transition metal (M): Ising type ordering in $FePS_3$ [21], Heisenberg type ordering in $MnPS_3$ [22] and XY-type ordering in $NiPS_3$ [23]. Among these, $FePS_3$ has attracted particular interest as Ising type magnetic ordering in the bulk $FePS_3$, which is stable in air [19], persists down to monolayer [21].

In bulk $FePS_3$ with monoclinic crystal structure (space group $C2/m$), each Fe^{2+} ion is bonded to six S^{2-} ions to form edge-sharing FeS_6 octahedra, while the Fe atoms form a honeycomb lattice. The S atoms are connected with two P atoms just above and below the Fe honeycomb plane which constitutes $(P_2S_6)^{4-}$ unit [21]. These arrangements are stacked along the c axis where each plane is bonded via very weak interlayer vdW interaction. The anisotropic magnetic behavior of the system is governed by the competing direct Fe-Fe exchange and indirect Fe-S-Fe superexchange interactions within layers (0.31 meV/cell), as well as by interlayer exchange interactions (1.41 meV/cell) [21].

Utilizing hydrostatic pressure as external stimuli and Raman scattering as an experimental probe to identify changes

*These authors contributed equally to this work.
†Contact author: sspsdd@iacs.res.in

in phonon modes of a 2D magnet in few-layers may facilitate the detection of correlated structural change in a progressive manner with enhancement of d-p metal-ligand charge transfer, and possible spin crossover (SCO) [24,25]. To the best of our knowledge, except the study on quantifying vdW interactions in the layered MoS_2 by measuring the valence-band maximum (VBM) splitting under pressure [26], the pressure-driven phase transition in few-layer vdW magnets have not yet been systematically investigated. The existing reports do not discount the effect of the third dimension in high-pressure studies on these 2D systems [24,27–29]. Consequently, the nature of volume collapse in finite-sized 2D materials, and the effect of the crystal field splitting with d^4–d^7 transition-metal-elements while reducing the sample thickness, and a possible concurrent insulator-metal transition (IMT) may add new scaling laws, originating from the dimensional effect, to the existing band theory of Mott insulators.

Herein, we methodically investigate room-temperature pressure-driven IMT in $FePS_3$ from the bulk (≈100 layers) to nearly 2D limit (≈3 layers) following characteristic phonon modes using micro-Raman scattering. Raman modes, compared with the first-principles density functional theory (DFT) calculations, reveal a thickness-dependent critical pressure (P_c) which reduces to 1.5 GPa in three-layer flakes compared with 10.8 GPa for the bulk counterpart. We have adopted a phenomenological model where a macroscopic structural change due to the variation of the effective in-plane strain with layer numbers may result in a reduction of the critical pressure in few-layer samples. Under applied pressure, few-layer flakes experience enhanced in-plane strain due to strong structural anisotropy which stipulates the decreasing effect of thickness on the critical pressure for IMT. Practically, interfacial adhesion in stacked vdW heterostructure or molecules trapped between layers can be used to realize pressure as low as 1–2 GPa [30]. The resulting conformational or magnetic changes can be investigated without use of intricate DAC methodology. Most importantly, engineered flakes can be employed in the conventional three-terminal field-effect transistor (FET) device architecture.

II. EXPERIMENTAL AND COMPUTATIONAL DETAILS

Bulk crystals of $FePS_3$ with 99.999% purity from 2D Semiconductors (USA) were used in the present study. Three types of $FePS_3$ samples, namely, thin-layer $FePS_3$ flakes, thick layer $FePS_3$ flakes, and bulk $FePS_3$, were investigated during the experiment. $FePS_3$ flakes were mechanically exfoliated from the bulk crystal using scotch tape. The exfoliated flakes were transferred onto the diamond anvil using a micromanipulator under an optical microscope such that the flakes were placed at the center of the diamond culet (Fig. S1 of the Supplemental Material [31]). A stainless-steel gasket was used as a sample holder. The gasket was indented to a thickness of 60 μm and a hole of 180 μm diameter was drilled at the center of indentation to create the sample chamber. A few ruby spheres were placed with the sample to determine the pressure inside the sample chamber during the experiment. The chamber was filled with methanol-ethanol mixed in 4 : 1 ratio which acted as a quasihydrostatic pressure transmitting medium (PTM). The flakes are not controlled in thickness and each flake contains areas with various thicknesses. The thickness of the target experimental area of a flake was estimated following previous experience as reported in the earlier studies [32,33]. The experiment was done in a Diacell Bragg-Mini diamond-anvil cell (DAC) with a culet diameter of 500 μm. Raman spectra were collected using a Horiba T64000 Raman setup. The spectra were taken in backscattering geometry using a DPSS laser ($\lambda = 532$ nm) as excitation source, and the beam was focused to a spot size of 1 μm by 50× long-distance objective (NA = 0.50). A constant laser power of around 5 mW was used throughout the experiment. We kept the temperature of the surroundings fixed during the experiment. Any small temperature change could not affect our ruby spectra within the spectral resolution of the Raman spectrometer. Hence the pressure values are mentioned up to the first decimal places with ±0.1GPa error. The consistency of Raman modes for a particular thickness was verified at different spots with similar contrast under an optical microscope.

All the spin-polarized calculations were performed within the framework of density functional theory (DFT) using the plane-wave technique as implemented in the Vienna ab initio simulation package (VASP) [34]. Further details of the computational studies are given in Supplemental Material (SM) [31].

III. EXPERIMENTAL AND COMPUTATIONAL RESULTS

High-pressure x-ray diffraction study on powder $FePS_3$ by Haines *et al.* [25] reported two structural phase transitions, the first transition pressure (PT1) at approximately 4 GPa and the second (PT2) at approximately 14 GPa. At the first transition pressure, an alignment of the vdW planes was predicted, where Fe atoms directly come above one another, and likewise for the P atoms. At PT2 the study observed dramatic volume collapse in the out-of-plane direction. The study also reported an insulator-to-metal transition at around 5 GPa in resistivity measurement on a single crystal. Similar structural evolution was observed by Jarvis *et al.* in x-ray diffraction study on powder and single crystal $FePS_3$ [35]. Furthermore, Wang *et al.*'s resistivity measurements on single crystalline $FePS_3$ and x-ray emission spectroscopy study showed the insulator-to-metal transition and spin state transition of Fe^{2+} ions at around 14 GPa, which was accompanied by a sudden volume collapse in high-pressure powder x-ray diffraction study [24]. The present study reports the first high-pressure Raman measurements on mechanically exfoliated vdW layers, here $FePS_3$, under quasihydrostatic pressure in an attempt to tune the transition pressure (PT1 as suggested by Haines *et al.* [25]) for the alignment of vdW planes depending on the layer numbers. The experimental observations for three different layer thicknesses have been corroborated by computational calculations.

Three types of $FePS_3$ samples were transferred on to the diamond culet: thin layer (≈3 layers), thick layer (≈30 layers) and bulk (more than 100 layers). Examples of the first two are shown in Fig. 1(a). Figure 1(b) depicts the image of the bulk sample (more than 100 layers) loaded inside the gasket hole in the DAC. In conclusion, substrate-free $FePS_3$ samples were directly loaded into the DAC to investigate the intrinsic properties of the two-dimensional systems, minimizing the effect of strain, substrate-material charge transfer, or optical

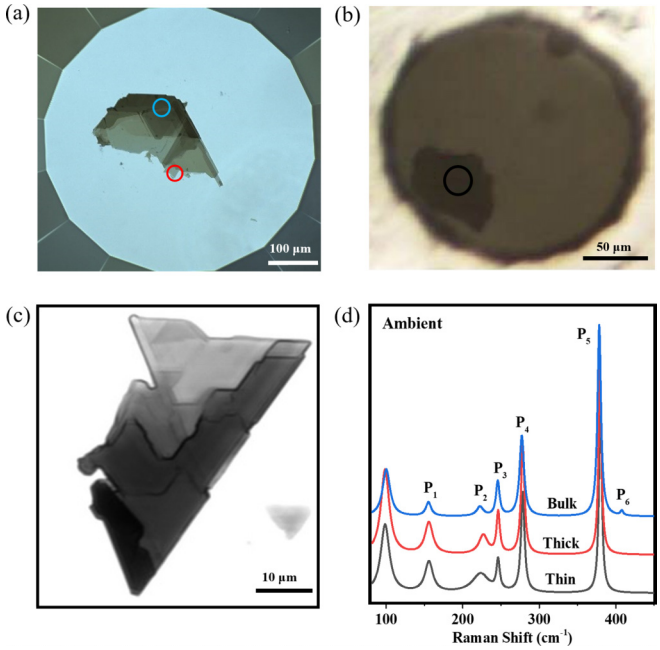

FIG. 1. Raman spectroscopy of $FePS_3$ flake on diamond culet: (a) Micrograph of an exfoliated flake on the diamond culet. Thin and thick areas are marked with red and blue circles, respectively. (b) Transferred bulk sample inside the loaded DAC marked with a black circle. (c) Optical micrograph in transmission mode of a typical exfoliated flake showing the contrast variation with change in layer number. (d) Room-temperature Raman spectra of the bulk, thick and thin layer $FePS_3$ on top of the diamond. Different phonon modes are labeled P_i ($i = 1$–6). A new weak mode P_6 is spotted at 407 cm^{-1}, which is not reported in the previous studies. P_6 is not clearly visible for thick and thin layers. The broad Raman mode around 105 cm^{-1} is a zone-folded phonon mode, as reported earlier [32].

interference. The approximate layer thickness of the transferred flakes has been determined from the intensity ratio of the Raman modes at 277 and 378 cm^{-1} [32,33,36]. This has been reconfirmed by an optical micrograph in transmission mode [Fig. 1(c)] of the exfoliated samples on diamond culet where darker contrast indicates a higher number of layers. Figure 1(d) shows the Raman spectra of the thin layer, thick layer, and bulk $FePS_3$ at room temperature, which is similar to the previous reports [21,27,37]. At ambient condition, $FePS_3$ adopts the $C2/m$ symmetry group, which has 30 vibrational modes at the Brillouin-zone center: $\Gamma = 8A_g + 6A_u + 7B_g + 9B_u$. Among these, the Raman-active A_g and B_g modes are observed in the Raman-scattering experiment. Previous Raman-scattering data on $FePS_3$ as reported by Wang *et al.* [24] identified the phonon symmetries of the observed modes P_1, P_2, and P_4 as A_g/B_g (156, 224, and 277 cm^{-1}) and P_3 and P_5 as A_g (246 and 378 cm^{-1}); these modes are due to molecule-like vibration from the $(P_2S_6)^{4-}$ bipyramid structure. The low-frequency peaks at 98 and 156 cm^{-1} are from the vibration of Fe atoms and the broadening of these modes is due to local fluctuation or disorder, as suggested by Lee *et al.* [21]. Another new weak peak detected for the bulk sample at 407 cm^{-1} (P_6) was not reported in previous studies. Apart from the diamond anvil, $FePS_3$ with different layer thicknesses have been transferred and characterized on SiO_2/Si substrate, *p*-Si, hBN, graphene and diamond thin films. The micro-Raman spectrum in each case contains the characteristic Raman modes discussed in this report. The individual peaks have finite shifts for different substrates, but importantly, the relative positions of the specific modes remain unchanged. Since the current study investigates the evolution of the Raman modes with pressure, the relevance of such substrate effect may be discounted.

In the bulk $FePS_3$, Fig. 2(a), with increasing pressure, the Raman spectra show a hardening of P_1 to P_6 up to 12.2 GPa. Note that P_2 at 224 cm^{-1} cannot be detected with considerable clarity. By 12.9 GPa, P_3 and P_4 disappear. The intensity of P_5 decreases and P_6 becomes more intense. With the application of pressure, all the detectable Raman peaks shift to higher frequencies because of the strengthening of intra-atom interactions under hydrostatic pressure. Unlike the other peaks, the frequency shift of the mode at 98 cm^{-1} with pressure has not been observed, rather a change in its shape is detected with the increasing pressure. The fact that all the modes seem to be broadening above 10 GPa, may be due to the hydrostatic limit of pressure transmitting medium [38]. P_3 and P_4 overlap and become difficult to be recognized beyond 12.2 GPa. The pressure-induced line broadening for all the peaks, along with the complete loss of Raman intensity can be attributed to pressure-driven metallization of $FePS_3$. Also, the evolution of the peak at 98 cm^{-1} under compression can be attributed to the gradual shift of the Fe atoms in the hexagon plane with pressure during the alignment of the vdW planes. The Raman modes for the bulk sample recover when the pressure is released [Fig. S2(a) of the SM [31]]. Concerning thick layer $FePS_3$ flake, in Fig. 2(b), all the characteristic Raman modes of $FePS_3$ can be identified, except the P_6 mode. Importantly, the Raman spectra exhibit the same trend as that observed in the bulk sample. Similar to the bulk sample, the broadening of all the Raman modes is observed above 10 GPa. While the pressure is released all the modes recovered around 3.6 GPa [Fig. S2(b) of the SM [31]].

Unlike bulk or thick sample, for the thin layered $FePS_3$, Fig. 2(c), P_1 and P_2 are very weak in intensity whereas the evolution of P_3, P_4, and P_5 characteristic modes can be observed with clarity. A similar trend in peak shift has been observed with increasing pressure, but, noticeably, the P_3 and P_4 modes become broad and asymmetric above 2 GPa. The asymmetric lineshape of the Raman spectra at the onset of metallization has also been observed for several other magnetic compounds [39–41]. Hence, the metallization of thin layer $FePS_3$ may initiate below 2 GPa. P_3, P_4, and P_5 disappear by 10 GPa, suggesting complete metallization of thin layer $FePS_3$. A broad peak persists between 300 and 370 cm^{-1} at high pressure. The P_3, P_4, and P_5 modes recover when the pressure is released, Fig. S2(c) of the SM [31]. The decrease of metallization pressure with decreasing thickness suggests interlayer interactions of $FePS_3$ opposing IMT. The P_6 mode is prominent above 12 GPa in the bulk sample and is not detected in thin and thick layered samples may be due to fewer vdW planes.

To study the pressure dependence of the Raman modes of the three samples, we fit each mode of the Raman spectra using Lorentzian lineshape function and plotted the peak positions of P_3, P_4, and P_5 modes with pressure in

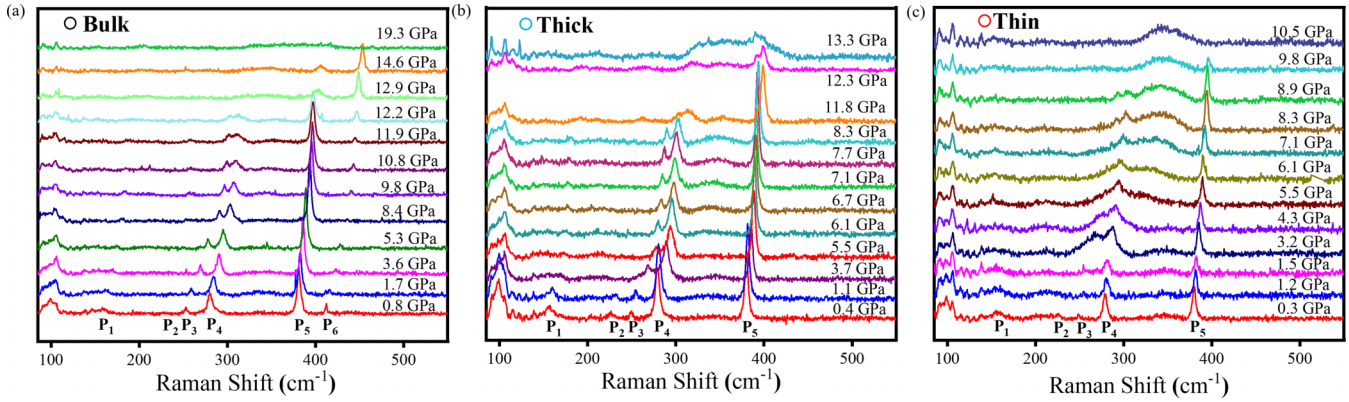

FIG. 2. Pressure dependent Raman spectroscopy of layered $FePS_3$: Pressure responses of Raman modes for (a) bulk, (b) thick and (c) thin $FePS_3$ flakes were recorded in a diamond anvil cell (DAC). All the modes P_i ($i = 1$–6) exhibit blueshift with increasing pressure. P_1 and P_2 are weak in intensity. Unlike the other peaks, with a change in pressure, the mode at 98 cm^{-1} does not shift, rather a change in its shape is detected for all three samples. For bulk samples, P_3 and P_4 modes disappear by 12.9 GPa. The intensity of P_5 decreases and P_6 becomes more intense. For thick layers, P_3 and P_4 become very broad at 11.8 GPa and difficult to detect after that. P_3 and P_4 modes become broad and asymmetric above 1.5 GPa for thin sample. P_3, P_4, and P_5 disappear below 10 GPa, and a broad peak between 300 and 370 cm^{-1} persists at high pressure.

Figs. 3(a)–3(c). The bulk, thick-, and thin-layer $FePS_3$ exhibit dissimilar trends in the pressure dependence of the Raman modes. Almost all the Raman modes disappear at different higher pressures. Before the modes disappear, a critical pressure separates the evolving trends of phonon modes for varying layer thicknesses. The DFT calculation is used to determine these critical pressures, and the results demonstrate a good match with the experimental observation, in which the phonon modes indeed exhibit a change in slope. Thus, three distinct regions—the low-pressure region (LP), the intermediate-pressure region (IP), and the high-pressure region—can be identified within the overall pressure evolution. The modes exhibit a linear increase in all three regions, and pressure-dependent linear blueshifts for all three samples in LP and IP zones are tabulated in Table I. The pressure-dependent blueshift of the Raman modes is larger in thin layered $FePS_3$ than in the thicker sample. A similar trend is observed for graphene [42,43] and TMDs [44] under pressure. For the thin layered sample, there are fewer vdW planes to buffer the pressure. Hence, more pronounced hardening of the vibrations and a higher rate of blueshift are observed. The rate of increase of P_3 mode with pressure is higher than P_4 and P_5 mode for all the considered cases. The different pressure dependence of mode shifts can be understood by analyzing the types of vibrations involved in these modes. The P_3 breathing mode involves out-of-plane vibration of sulfur atoms, whereas

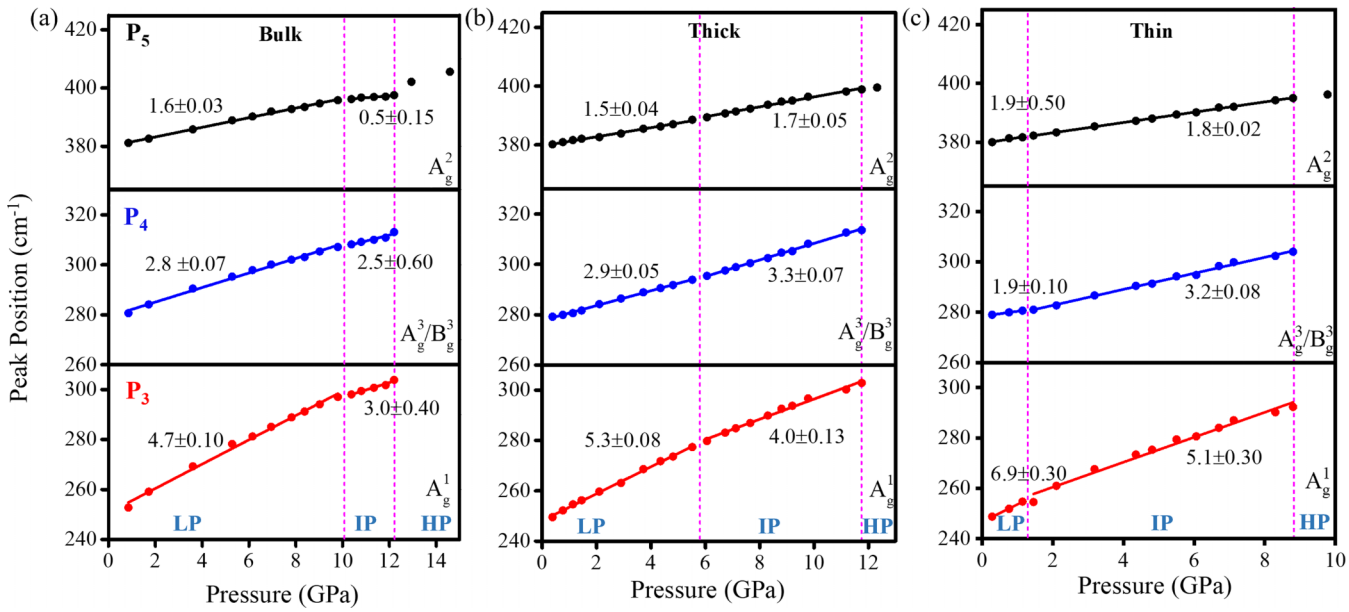

FIG. 3. Pressure evolution of phonon modes with different layer numbers: Panels (a), (b) and (c) show the change in peak positions of P_3, P_4, and P_5 modes for bulk, thick and thin layered $FePS_3$, respectively. A critical pressure delineates the evolving trends in phonon modes across various layer thicknesses before the Raman modes disappear. DFT calculations along with experimental observations, determines the critical pressures and specifies the distinct pressure regions: low-pressure (LP), intermediate-pressure (IP), and high-pressure (HP) zones.

TABLE I. Rate of change of peak shifts for the phonon modes P_3, P_4, and P_5 with pressure for bulk, thick and thin samples: The slopes (cm^{-1}/GPa) are calculated using linear fit for each sample and are mentioned for the low pressure (LP) and the intermediate pressure (IP) zones in the table. Pressure windows in two zones for the three samples are indicated in the parentheses in units of GPa.

Raman modes	LP zone			IP zone		
	Bulk (up to 10.8)	Thick (up to 6.1)	Thin (up to 1.5)	Bulk (10.8–12.9)	Thick (6.1–12.3)	Thin (1.5–8.9)
P_3	4.7 ± 0.1	5.3 ± 0.1	6.9 ± 0.3	3.0 ± 0.4	4.0 ± 0.1	5.1 ± 0.3
P_4	2.8 ± 0.1	2.9 ± 0.1	1.9 ± 0.1	2.5 ± 0.6	3.3 ± 0.1	3.2 ± 0.1
P_5	1.6 ± 0.1	1.5 ± 0.1	1.9 ± 0.5	0.5 ± 0.2	1.7 ± 0.1	1.8 ± 0.1

P_5 originates from symmetric stretching vibration of the P-S bonds and P_4 mode corresponds to in-plane stretching of P_2S_6 cluster [37,45]. With increasing pressure, the compression of out-of-plane P_3 mode becomes more favorable than the in-plane P_4 and P-S bonds stretching P_5 mode. Furthermore, in the case of bulk sample spectral separation between P_5 and P_6 increases with the pressure as it strengthens the out-of-plane P-P stretching P_6 vibration.

To rationalize the pressure-driven electronic phase transition as well as spin state transition, we have performed electronic structure calculations based on first-principles density functional theory (DFT) using the Vienna ab initio simulation package (VASP). The in-plane lattice parameters as well as interatomic distances decrease as pressure increases (Table S1 of the SM [31]). In addition, the calculated magnetic moment of Fe atom (3.34 μB) at 0 GPa [21,46,47] indicates that Fe^{2+} ions in bulk $FePS_3$ are in a high spin state ($S = 2$) while the gradual increase of external pressure on $FePS_3$ leads to a spin-crossover from high spin state (HS) to low spin state (LS) where $S = 0$. This spin-state transition can be distinctly observed from the calculated magnetic moment value which decreases with the increase in pressure and finally becomes 0.00 μB/Fe-atom at the spin-state transition pressure of 10.80 GPa (Table S1 of the SM [31]). The computational results indicate spin crossover at the onset of metallization which is in line with the theoretical prediction by Zheng *et al.* [46]. Also, the x-ray emission spectroscopy study by Wang *et al.* observed the collapse of Fe moment in the metallic phase suggesting spin crossover [24]. On the other hand, Coak *et al.*'s neutron powder diffraction experiment found persistent short-range magnetic orders that survive above room temperature where the Fe moment is similar to that at ambient pressure [48]. However, in the current study, the SCO is solely based on DFT calculations which also predict insulator-to-metal transition at the same critical pressure with layer number dependency. Even though the computational study found cooperative behavior of metallization and SCO, the current spectroscopic measurements cannot conclude the same. The explanation of these contradictory results with previous experimental studies is beyond the scope of the current experiment. In conclusion, this needs further investigation to resolve the unambiguousness of SCO in this type of system.

Bulk $FePS_3$ at 10.80 GPa undergoes a considerable decrease of in-plane lattice parameters ($a = 5.65$ Å, $b = 9.75$ Å), especially the Fe-S distance, indicating strain-induced lattice deformation and structural transition (Table S1 of the SM [31]). The density of states (DOS) analysis shn in Fig. S3(c) of the SM [31] vividly exhibits that bulk $FePS_3$ at 0 GPa is an insulator with a band gap (E_g) of 1.3 eV while the band gap narrows down with the increase of pressure and finally transforms into a metallic phase ($E_g = 0.00$ eV) at 10.80 GPa indicating insulator-to-metal phase transition (as the PBE functional highly underestimates the band gap [49], band gaps were not determined from band structure calculation). The local and projected density of states (LDOS and PDOS) analysis further justifies the pressure-driven spin-crossover in bulk $FePS_3$. At $P = 0$ GPa, both the LDOS and PDOS of the Fe atom demonstrate the asymmetric nature of electronic density of states for up and down spin, whereas, at the transition pressure (10.80 GPa), the profile eventually becomes symmetric, indicating spin pairing associated with the spin state transition [Figs. S3(d)–S2(f) of the SM [31]].

Furthermore, we have computed Raman spectra unveiling the optical phonon-property of bulk $FePS_3$ under pressure [Fig. S3(g) of the SM [31]]. Besides, the broadening and shifting of Raman peaks, two new peaks were generated at 326 and 342 cm^{-1} due to structural distortion arising from the shift of Fe atoms in the hexagonal plane along with P atoms resulting change in the alignment of vdW planes at transition pressure [Figs. S3(h) and S3(i) of the SM [31]]. This structural change of bulk $FePS_3$ as well as the generation of new Raman peaks above 10 GPa is in line with the earlier studies [21,25,47,48]. Hence, calculated Raman spectra further correlate the structural transition of bulk $FePS_3$ during spin state transition at 10.80 GPa.

Similar pressure-induced lattice distortion, as well as structural transition, is also observed for the thick [Figs. S4(a) and S4(b) of the SM [31]] and thin layer $FePS_3$ [Figs. S5(a) and S5(b) of the SM [31]]. The substantial change in in-plane lattice parameters and distance of Fe-S has similarly been observed here (Table S1 of the SM [31]). However the structural evolution is solely from DFT calculation and needs to be further analyzed experimentally on exfoliated $FePS_3$ layers. For thick [Fig. S4(c) of the SM [31]] and thin layer $FePS_3$ [Fig. 4(a)], DOS analysis demonstrates that the band gap narrows down with the increase of pressure and finally transforms into a metallic phase ($E_g = 0.00$ eV) at 6.06 and 1.45 GPa, respectively, indicating an insulator-to-metal phase transition. Also from the LDOS and PDOS analysis, unlike the bulk, the thick [Figs. S4(d)–S4(f) of the SM [31]] and thin layer $FePS_3$ [Figs. 4(b) and S5(d)–S5(f) of the SM [31]] demonstrate the spin-state transition accompanying the insulator-metal transition at a relatively low external pressure of 6.06 and 1.45 GPa, respectively. Both the thick [Fig. S4(g) of the SM [31]] and

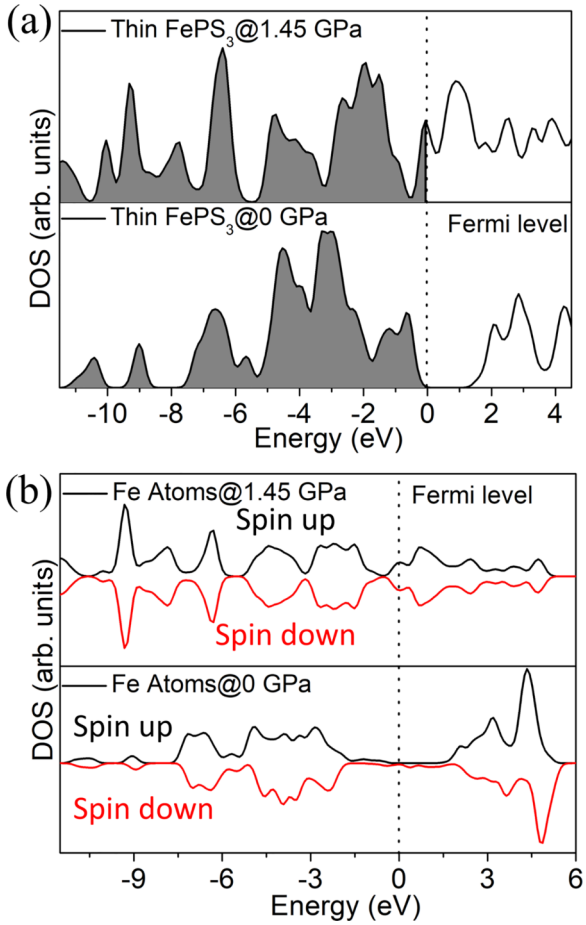

FIG. 4. Density of states (DOS) calculations for $FePS_3$: (a) Total density of states (TDOS) and (b) localized density of states (LDOS) of Fe atom for monolayer $FePS_3$ (thin sample). The asymmetric nature of the electronic density of states for up and down spins in LDOS eventually becomes symmetrical at a certain critical pressure, 1.45 GPa, where the band gap reduces to zero, which indicates the transition of the spin state of Fe^{2+} ion from $S = 2$ to $S = 0$. The critical pressure for both TDOS and LDOS studies increases with increasing layer numbers as shown in Figs. S4(c) and S4(d) of the SM [31] for thick (6.06 GPa) and Figs. S3(c) and S3(d) of the SM [31] for bulk sample (10.48 GPa).

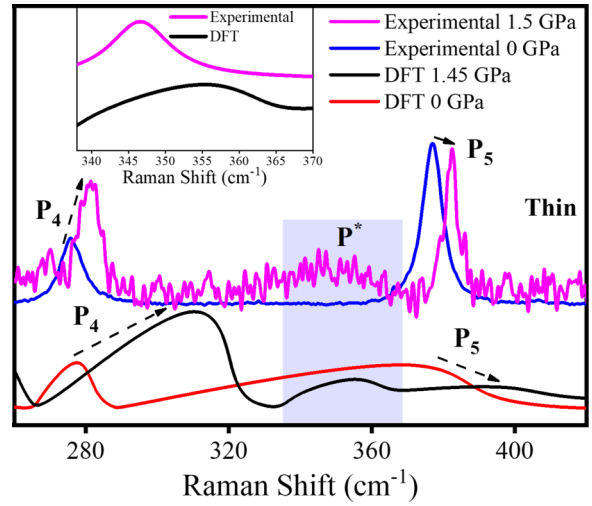

FIG. 5. Experimental and computational Raman spectra for thin layer $FePS_3$: Dashed arrows highlight that both Raman spectra show a hardening of P_4 and P_5 modes with an increase in pressure. The evolution of the new peak P^* in the computational studies specified by the shaded region at the critical pressure can be mapped to the broad weak peak that evolves in the experimental high-pressure Raman spectra between P_4 and P_5. Inset shows a comparative depiction of P^* mode in the shaded region of the experimental (at 1.5 GPa) and computational spectra (at 1.45 GPa).

thin layer [Fig. S5(g) of the SM [31]] $FePS_3$ exhibit similar Raman spectra under pressure except the higher frequency A_g mode beyond 410 cm^{-1} which is suppressed here in contrast with bulk $FePS_3$. A Raman mode P^* evolves between 300 to 370 cm^{-1} in the computational study for the bulk [Figs. S3(h) and S3(i) of the SM [31]], thick [Figs. S4(h) and S4(i) of the SM [31]] and thin [Figs. S5(h) and S5(i) of the SM [31]] samples around the critical pressure at which the computed band gap reduces to zero. The calculated critical pressures for thin, thick, and bulk samples match the onset of the IP region (Fig. 3) in experimental Raman spectra. The evolution of this new peak P^* in the computational studies can be mapped to the broad weak peak that evolves in the experimental high-pressure Raman spectra between P_4 and P_5 for all three samples (Fig. S6). P^* and the calculated magnetic moments for the three samples are represented in Fig. S7 of the SM [31]. Unlike in the bulk sample, the evolution of P^* is more prominent in thin and thick samples due to less intense neighboring phonon modes. Figure 5 depicts the comparative evolution of this broad phonon mode P^* and the hardening of P_4 and P_5 modes in both experimental and computational Raman spectra for the thin flake. Similarly, for bulk and thick, see Fig. S6 of the SM [31] P^* may be a convolution of M4 to M8 modes observed in the high-pressure Raman study of $FePS_3$ in a thin crystalline pallet by Das *et al.* [47] and was also supported by their theoretical calculation of Raman modes. The origin of this envelope requires further investigation.

IV. DISCUSSION

Using current computational studies and previous works on the same sample under external pressure, three distinct zones (LP, IP, HP) can be detected in the pressure dependence of Raman modes (Fig. 3). The pressure-driven metallization and spin-crossover of the Fe^{2+} ion from $S = 2$ ($t_{2g}^4 e_g^2$) to $S = 0$ ($t_{2g}^6 e_g^0$) observed in the computational studies predicts an enhancement of *d-p* metal-ligand hybridization which is almost at the onset of the experimental IP region. This indicates that the experimental IP region might be viewed as the beginning of the metallic phase which was previously described as a semiconducting phase by Zheng *et al.* in their computational study [46]. Also, the IP region could be considered to be a bad metal, as predicted by Kim *et al.*, where the IMT is mediated by t_{2g} orbital of Fe^{2+} ion, leaving e_g gapped [50]. Importantly, this IP region involves a structural change where weak vdW force favors slippage between layers [26]. Consequently, a sudden slippage among the layers takes place where the crystallographic *c* axis becomes perpendicular to the *ab* plane and Fe atoms in one layer are placed exactly

above the adjacent layer [25,46]. It may be anticipated that this particular sliding will require higher pressure for a large number of layers under hydrostatic consideration. Because of this, as the number of layers decreases, the transition pressure for this initial structural phase transition that leads to the IMT will also decrease. On the other hand, at the beginning of the HP zone, an experimentally observed sudden volume collapse by Haines *et al.* and Wang *et al.* is accompanied by the creation of an in-plane Fe-Fe intermetallic bonding, which delocalizes electrons [24,25]. Thus, a complete metallization takes place in this regime followed by the Raman mode collapse in the micro Raman study.

To understand our results concerning the layer-dependent phase transition from the macroscopic viewpoint, any 2D stacking can be conceptualized as thin sheets experiencing anisotropic strain under hydrostatic pressure consideration (Fig. S8 of the SM [31]). In this configuration, each layer or sheet encounters the same amount of force F_t along the transverse direction. On the other hand, the force acting along the stairs will be equally distributed among all of the sheets (effective force, $F_{\text{eff}} = F_l/N$, N is the number of sheets). As a result, when the same amount of pressure is acting among all three directions, the out-of-plane strain will be thickness invariant, but the in-plane strain will be larger with fewer sheets since it is inversely proportional to the layer numbers. Thus, it may be anticipated that any structural transition involving in-plane deformation will hold for a smaller number of sheets at a substantially lower external pressure. Interestingly, our experimental results justify the above argument if we consider the first transition point for the $FePS_3$ flakes which occurs at lower pressure for the thin layered samples (1.5 GPa for thin and 10.8 GPa for the bulk). Furthermore, around this pressure, if the effective in-plane strain is high enough for substantial orbital overlap, metallic behavior may initiate in the sample. As a result, the transition from insulator to metal for thin layers will occur at a lower external pressure than that for thicker samples. Furthermore, from the microscopic viewpoint, an electronic Hubbard model can be introduced by considering the spectral range (bandwidth W) as a function of layer number N and pressure P with power-law scaling, which suggests IMT at relatively low pressure for a few-atomic layer flake (see the Supplemental Material [31]).

V. CONCLUSIONS

In conclusion, layer dependence of the critical pressure for the spin-crossover and the insulator-to-metal transition in a layered vdW magnet, $FePS_3$, has been systematically investigated via micro-Raman spectroscopy, supported by the first-principles DFT calculations. DFT calculations along with experimental observations determine the three distinct pressure regimes which reflect different trends in phonon modes across layer thicknesses. Detailed analysis of the computational results shows the SCO from a high ($S = 2$) to low spin state ($S = 0$) with a thickness-dependent critical pressure P_c which reduces to 1.5 GPa in three-layer flakes compared with 10.8 GPa for the bulk counterpart. Although the disappearance of Raman modes in the experimental data indicates complete metallization at the high-pressure zone, computational studies suggest that IMT may be initiated with the metal-ligand charge transfer at much lower pressure. A phenomenological model explained that structurally anisotropic $FePS_3$ flake experiences more in-plane strain with decreasing layer numbers at a fixed pressure. The electronic Hubbard model, where the layer number dependence in the form of power-law scaling is introduced along with pressure in the bandwidth, suggests the IMT at relatively low pressure for a few-atomic layer flake. The possibility of realizing 1–2 GPa in functional vdW materials with interfacial adhesion [30] or adapting chemical pressure [51] may open up alternative strategies (see Supplemental Material [31]) toward exploring novel phases in atomic-layer magnets for spintronic devices applications.

ACKNOWLEDGMENTS

The authors would like to thank Goutam Dev Mukherjee, Sanjay Kumar, and Anand Kumar for their technical help during the high-pressure experiments. The financial support (fellowships) from IACS, DST-INSPIRE, and CSIR-UGC are greatfully acknowledged. S. Datta acknowledges the financial support from DST-SERB Grant No. CRG/2021/004334. S. Datta also acknowledges the technical research center, IACS. A.D. thanks SERB Grant No. CRG/2020/000301 for partial funding.

S. Datta and B.M. conceived the project and designed the experiments. A.G. and S.M. prepared the samples and performed the initial characterization. B.M., S. Datta, and S.J. initiated the experiments at JNCASR taking inputs from C.N. Furthermore, M.P., S. Das, T.K., and S.M. carried out the pressure-dependent studies at IACS and confirmed the results. All DFT calculations were performed by R.J. with the inputs from A.D. S. Das and S. Datta developed the analytical model. All authors discussed the results and actively commented on the paper written by M.P., S. Das, B.M., R.J., and S. Datta.

[1] K. Mak, C. Lee, J. Hone, J. Shan, and T. F. Heinz, Atomically thin MoS_2: A new direct-gap semiconductor, Phys. Rev. Lett. **105**, 136805 (2010).

[2] Q. H. Wang, K. Kalantar-Zadeh, A. Kis, J. N. Coleman, and M. S. Strano, Electronics and optoelectronics of two-dimensional transition metal dichalcogenides, Nat. Nanotechnol. **7**, 699 (2012).

[3] S. Tongay, J. Zhou, C. Ataca, K. Lo, T. S. Matthews, J. Li, J. C. Grossman, and J. Wu, Thermally driven crossover from indirect toward direct bandgap in 2D semiconductors: $MoSe_2$ versus MoS_2, Nano Lett. **12**, 5576 (2012).

[4] S. Dai, Z. Fei, Q. Ma, A. S. Rodin, M. Wagner, A. S. McLeod, M. K. Liu, W. Gannett, W. Regan, K. Watanabe, T. Taniguchi, M. Thiemens, G. Dominguez, A. H. C. Neto, A. Zettl, F. Keilmann, P. Jarillo-Herrero, M. M. Fogler, and D. N. Basov, Tunable phonon polaritons in atomically thin van der Waals crystals of boron nitride, Science **343**, 1125 (2014).

[5] Y. Liu, X. Hua, C. Xiao, T. Zhou, P. Huang, Z. Guo, B. Pan, and Y. Xie, Heterogeneous spin states in ultrathin nanosheets induce subtle lattice distortion to trigger efficient hydrogen evolution, J. Am. Chem. Soc. **138**, 5087 (2016).

[6] A. P. Nayak, T. Pandey, D. Voiry, J. Liu, S. T. Moran, A. Sharma, C. Tan, C. Chen, L. Li, M. Chhowalla, J. Lin, A. K. Singh, and D. Akinwande, Pressure-dependent optical and vibrational properties of monolayer molybdenum disulfide, Nano Lett. **15**, 346 (2015).

[7] A. K. Geim and I. V. Grigorieva, Van der Waals heterostructures, Nature (London) **499**, 419 (2013).

[8] K. S. Novoselov, A. Mishchenko, A. Carvalho, and A. H. C. Neto, 2D materials and van der Waals heterostructures, Science **353**, 9439 (2016).

[9] S. A. Wolf, D. D. Awschalom, R. A. Buhrman, J. M. Daughton, S. von Molnar, M. L. Roukes, A. Y. Chtchelkanova, and D. M. Treger, Spintronics: A spin-based electronics vision for the future, Science **294**, 1488 (2001).

[10] T. Jungwirth, X. Marti, P. Wadley, and J. Wunderlich, Antiferromagnetic spintronics, Nat. Nanotechnol. **11**, 231 (2016).

[11] H. Ito, T. Asai, Y. Shimizu, H. Hayama, Y. Yoshida, and G. Saito, Pressure-induced superconductivity in the antiferromagnet $\kappa(ET)_2CF_3SO_3$ with quasi-one-dimensional triangular spin lattice, Phys. Rev. B **94**, 020503(R) (2016).

[12] Y. Ma, Y. Dai, M. Guo, C. Niu, Y. Zhu, and B. Huang, Evidence of the existence of magnetism in pristine VX_2 monolayers (X = S, Se) and their strain-induced tunable magnetic properties, ACS Nano **6**, 1695 (2012).

[13] S. Lebegue, T. Bjorkman, M. Klintenberg, R. M. Nieminen, and O. Eriksson, Two-dimensional materials from data filtering and Ab Initio calculations, Phys. Rev. X **3**, 031002 (2013).

[14] N. Sivadas, M. W. Daniels, R. H. Swendsen, S. Okamoto, and Di Xiao, Magnetic ground state of semiconducting transition-metal trichalcogenide monolayers, Phys. Rev. B **91**, 235425 (2015).

[15] H. L. Zhuang, Y. Xie, P. R. C. Kent, and P. Ganesh, Computational discovery of ferromagnetic semiconducting single-layer $CrSnTe_3$, Phys. Rev. B **92**, 035407 (2015).

[16] W. Zhang, Q. Qu, P. Zhua, and C. Lam, Robust intrinsic ferromagnetism and half semiconductivity in stable two-dimensional single-layer chromium trihalides, J. Mater. Chem. C **3**, 12457 (2015).

[17] L. J. Sandilands, J. X. Shen, G. M. Chugunov, S. Y. F. Zhao, Shimpei Ono, Y. Ando, and K. S. Burch, Stability of exfoliated $Bi_2Sr_2Dy_xCa_{1-x}Cu_2O_{8+\delta}$ studied by Raman microscopy, Phys. Rev. B **82**, 064503 (2010).

[18] C. Kuo, M. Neumann, K. Balamurugan, H. J. Park, S. Kang, H. W. Shiu, J. H. Kang, B. H. Hong, M. Han, T. W. Noh, and J.-G. Park, Exfoliation and Raman spectroscopic fingerprint of few-layer $NiPS_3$ van der Waals crystals, Sci. Rep. **6**, 20904 (2016).

[19] K. Du, X. Wang, Y. Liu, P. Hu, M. I. B. Utama, C. K. Gan, Q. Xiong, and C. Kloc, Weak van der Waals stacking, wide-range band gap, and Raman study on ultrathin layers of metal phosphorus trichalcogenides, ACS Nano **10**, 1738 (2016).

[20] Y. Tian, M. J. Gray, H. Ji, R. J. Cava, and K. S. Burch, Magneto-elastic coupling in a potential ferromagnetic 2D atomic crystal, 2D Mater. **3**, 025035 (2016).

[21] J. Lee, S. Lee, J. H. Ryoo, S. Kang, T. Y. Kim, P. Kim, C. Park, J.-G. Park, and H. Cheong, Ising-type magnetic ordering in atomically thin $FePS_3$, Nano Lett. **16**, 7433 (2016).

[22] Y. Sun, Q. Tan, X. Liu, Y. Gao, and J. Zhang, Probing the magnetic ordering of antiferromagnetic $MnPS_3$ by Raman spectroscopy, J. Phys. Chem. Lett. **10**, 3087 (2019).

[23] A. R. Wildes, V. Simonet, E. Ressouche, G. J. McIntyre, M. Avdeev, E. Suard, S. A. J. Kimber, D. Lancon, G. Pepe, B. Moubaraki, and T. J. Hicks, Magnetic structure of the quasi-two-dimensional antiferromagnet $NiPS_3$, Phys. Rev. B **92**, 224408 (2015).

[24] Y. Wang, J. Ying, Z. Zhou, J. Sun, T. Wen, Y. Zhou, N. Li, Q. Zhang, F. Han, Y. Xiao, P. Chow, W. Yang, V. V. Struzhkin, Y. Zha, and H. Mao, Emergent superconductivity in an iron-based honeycomb lattice initiated by pressure-driven spin-crossover, Nat. Commun. **9**, 1914 (2018).

[25] C. R. S. Haines, M. J. Coak, A. R. Wildes, G. I. Lampronti, C. Liu, P. Nahai Williamson, H. Hamidov, D. Daisenberger, and S. S. Saxena, Pressure-induced electronic and structural phase evolution in the van der Waals compound $FePS_3$, Phys. Rev. Lett. **121**, 266801 (2018).

[26] P. Ci, Y. Chen, J. Kang, R. Suzuki, H. S. Choe, J. Suh, C. Ko, T. Park, K. Shen, Y. Iwasa, S. Tongay, J. W. Ager, L.-W. Wang, and J. Wu, Quantifying van der Waals interactions in layered transition metal dichalcogenides from pressure-enhanced valence band splitting, Nano Lett. **17**, 4982 (2017).

[27] X. Wang, K. Du, Y. Y. F. Liu, P. Hu, J. Zhang, Q. Zhang, M. H. S. Owen, X. Lu, C. K. Gan, P. Sengupta, C. Kloc, and Q. Xiong, Raman spectroscopy of atomically thin two-dimensional magnetic iron phosphorus trisulfide ($FePS_3$) crystals, 2D Mater. **3**, 031009 (2016).

[28] I. Breslavetz, A. Delhomme, T. Pelini, A. Pawbake, D. Vaclavkova, M. Orlita, M. Potemski, M.-A. Measson, and C. Faugeras, Spatially resolved optical spectroscopy in extreme environment of low temperature, high magnetic fields and high pressure, Rev. Sci. Instrum. **92**, 123909 (2021).

[29] A. Pawbake, T. Pelini, A. Delhomme, D. Romanin, D. Vaclavkova, G. Martinez, M. Calandra, M.-A. Measson, M. Veis, M. Potemski, M. Orlita, and C. Faugeras, High-pressure tuning of magnon-polarons in the layered antiferromagnet $FePS_3$, ACS Nano **16**, 12656 (2022).

[30] K. S. Vasu, E. Prestat, J. Abraham, J. Dix, R. J. Kashtiban, J. Beheshtian, J. Sloan, P. Carbone, M. Neek-Amal, S. J. Haigh, A. K. Geim, and R. R. Nair, Van der Waals pressure and its effect on trapped interlayer molecules, Nat. Commun. **7**, 12168 (2016).

[31] See Supplemental Material at http://link.aps.org/supplemental/10.1103/PhysRevB.109.235417 for the details of computational methods and other figures, which includes Refs. [52–58].

[32] A. Ghosh, M. Palit, S. Maity, V. Dwij, S. Rana, and S. Datta, Spin-phonon coupling and magnon scattering in few-layer antiferromagnetic $FePS_3$, Phys. Rev. B **103**, 064431 (2021).

[33] D. Vaclavkova, M. Palit, J. Wyzula, S. Ghosh, A. Delhomme, S. Maity, P. Kapuscinski, A. Ghosh, M. Veis, M. Grzeszczyk, C. Faugeras, M. Orlita, S. Datta, and M. Potemski, Magnon polarons in the van der Waals antiferromagnet $FePS_3$, Phys. Rev. B **104**, 134437 (2021).

[34] G. Kresse and J. Hafner, *Ab initio* molecular dynamics for liquid metals, Phys. Rev. B **47**, 558(R) (1993).

[35] D. M. Jarvis, M. J. Coak, H. Hamidov, C. R. S. Haines, G. I. Lampronti, C. Liu, S. Deng, D. Daisenberger, D. R. Allan, M. R. Warren, A. R. Wildes, and S. S. Saxena, Comparative structural evolution under pressure of powder and single crystals of the layered antiferromagnet $FePS_3$, Phys. Rev. B **107**, 054106 (2023).

[36] H. Xu, S. Wang, J. Ouyang, X. He, H. Chen, Y. Li, Y. Liu, R. Chen, and J. Yang, Surface modification of multilayer $FePS_3$ by Ga ion irradiation, Sci. Rep. **9**, 15219 (2019).

[37] M. Scagliotti, M. Jouanne, M. Balkanski, G. Ouvrard, and G. Benedek, Raman scattering in antiferromagnetic $FePS_3$ and $FePSe_3$ crystals, Phys. Rev. B **35**, 7097 (1987).

[38] S. Klotz, J.-C. Chervin, P. Munsch, and G. L. Marchand, Hydrostatic limits of 11 pressure transmitting media, J. Phys. D: Appl. Phys. **42**, 075413 (2009).

[39] D. Marrocchelli, P. Postorino, D. Di Castro, E. Arcangeletti, P. Dore, M. Cestelli Guidi, S. Ray, and D. D. Sarma, Pressure and temperature dependence of the Fano resonance in the Raman spectrum of A_2FeMoO_6 systems (A = Sr, Ca), Phys. Rev. B **76**, 172405 (2007).

[40] J. L. Her, H. L. Liu, C. H. Shen, R. S. Liu, and H. S. Sheu, Effect of Ca doping on the optical properties of $La_{1.2}Sr_{1.8}Mn_2O_7$, J. Appl. Phys. **99**, 1013905 (2006).

[41] M. Baldini, V. V. Struzhkin, A. F. Goncharov, P. Postorino, and W. L. Mao, Persistence of Jahn-Teller distortion up to the insulator to metal transition in $LaMnO_3$, Phys. Rev. Lett. **106**, 066402 (2011).

[42] J. E. Proctor, E. Gregoryanz, K. S. Novoselov, M. Lotya, J. N. Coleman, and M. P. Halsall, High-pressure Raman spectroscopy of graphene, Phys. Rev. B **80**, 073408 (2009).

[43] K. Filintoglou, N. Papadopoulos, J. Arvanitidis, D. Christofilos, O. Frank, M. Kalbac, J. Parthenios, G. Kalosakas, C. Galiotis, and K. Papagelis, Raman spectroscopy of graphene at high pressure: Effects of the substrate and the pressure transmitting media, Phys. Rev. B **88**, 045418 (2013).

[44] X. Cheng, Y. Li, J. Shang, C. Hu, Y. Ren, M. Liu, and Z. Qi, Thickness-dependent phase transition and optical behaviour of MoS_2 films under high pressure, Nano Res. **11**, 855 (2018).

[45] M. Bernasconi, G. L. Marra, G. Benedek, L. Miglio, M. Jouanne, C. Julien, M. Scagliotti, and M. Balkanski, Lattice dynamics of layered MPX_3 (M = Mn, Fe, Ni, Zn; X = S, Se) compounds, Phys. Rev. B **38**, 12089 (1988).

[46] Y. Zheng, X. Jiang, X. Xue, J. Dai, and Y. Feng, *Ab initio* study of pressure-driven phase transition in $FePS_3$ and $FePSe_3$, Phys. Rev. B **100**, 174102 (2019).

[47] S. Das, S. Chaturvedi, D. Tripathy, S. Grover, R. Singh, D. V. S. Muthu, S. Sampath, U. V. Waghmare, and A. K. Sood, Raman and first-principles study of the pressure-induced Mott-insulator to metal transition in bulk $FePS_3$, J. Phys. Chem. Solids **164**, 110607 (2022).

[48] M. J. Coak, D. M. Jarvis, H. Hamidov, A. R. Wildes, J. A. M. Paddison, C. Liu, C. R. S. Haines, N. T. Dang, S. E. Kichanov, B. N. Savenko, S. Lee, M. Kratochvilova, S. Klotz, T. C. Hansen, D. P. Kozlenko, J.-G. Park, and S. S. Saxena, Emergent magnetic phases in pressure-tuned van der Waals antiferromagnet $FePS_3$, Phys. Rev. X **11**, 011024 (2021).

[49] J. P. Perdew and M. Levy, Physical content of the exact Kohn-Sham orbital energies: Band gaps and derivative discontinuities, Phys. Rev. Lett. **51**, 1884 (1983).

[50] M. Kim, H.-S. Kim, K. Haule, and D. Vanderbilt, Orbital-selective Mott phase and non-Fermi liquid in $FePS_3$, Phys. Rev. B **105**, L041108 (2022).

[51] E. O. Gomes, A. F. Gouveia, L. Gracia, Á. Lobato, J. M. Recio, and J. Andrés, A chemical-pressure-induced phase transition controlled by lone electron pair activity, J. Phys. Chem. Lett. **13**, 9883 (2022).

[52] F. Datchi, A. Dewaele, P. Loubeyre, R. Letoullec, Y. L. Godec, and B. Canny, Optical pressure sensors for high-pressure-high-temperature studies in a diamond anvil cell, High Pressure Res. **27**, 447 (2007).

[53] J. P. Perdew, K. Burke, and M. Ernzerhof, Generalized gradient approximation made simple, Phys. Rev. Lett. **77**, 3865 (1996).

[54] S. Grimme, Semiempirical GGA type density functional constructed with a long range dispersion correction, J. Comput. Chem. **27**, 1787 (2006).

[55] D. Porezag and M. R. Pederson, Infrared intensities and Raman scattering activities within density functional theory, Phys. Rev. B **54**, 7830 (1996).

[56] A. Fonari and S. Stauffer, vasp_raman.py, https://github.com/raman-sc/VASP/ (2013).

[57] S. G. Ovchinnikov, Effect of spin crossovers on the Mott-Hubbard transition at high pressures, J. Exp. Theor. Phys. **107**, 140 (2008).

[58] G. Shen, Y. Wang, A. Dewaele, C. Wu, D. E. Fratanduono, J. Eggert, S. Klotz, K. F. Dziubek, P. Loubeyre, O. V. Fat'yanov, P. D. Asimow, T. Mashimo, R. M. M. Wentzcovitch, and other members of the IPPS task group, Toward an international practical pressure scale: A proposal for an IPPS ruby gauge (IPPS-Ruby2020), High Pressure Res. **40**, 299 (2020).